EEG Biometrics for Individual Recognition in Resting State with Closed Eyes

Daria La Rocca(*), Patrizio Campisi(*), Gaetano Scarano(**)

*Department of Applied Electronics
Università degli Studi "Roma Tre"
via Della Vasca Navale 84,
I-00146 Roma, Italy
dlarocca@uniroma3.it
campisi@uniroma3.it

** DIET
Sapienza Università di Roma
via Eudossiana 18,
I-00184 Roma, Italy
gaetano.scarano@uniroma1.it

Abstract: In this paper EEG signals are employed for the purpose of automatic user recognition. Specifically the resting state with closed eyes acquisition protocol has been here used and deeply investigated by varying the employed electrodes configuration both in number and location for optimizing the recognition performance still guaranteeing sufficient user convenience. A database of 45 healthy subjects has been employed in the analysis. Autoregressive stochastic modeling and polynomial regression based classification has been applied to extracted brain rhythms in order to identify the most distinctive contributions of the different subbands in the recognition process. Our analysis has shown that significantly high recognition rates, up to 98.73%, can be achieved when using proper triplets of electrodes, which cannot be achieved by employing couple of electrodes, whereas sets of five electrodes in the central posterior region of the scalp can guarantee very high recognition performance while limiting user convenience.

这个准确率用三导联可以实现，二导联无法达到

1 Introduction

EEG recordings can be investigated in terms of rhythmic activity, and it has been shown that considering specific frequency bands can lead to analyze brain functions related to some assigned tasks [Baş99]. In this context, the so called "brain oscillations" have been analyzed from the beginning of EEG research, when the German neurophysiologist Berger ([Ber29]) first observed the dominant oscillations of approximately 10 Hz. In general, five main widely studied rhythms can be revealed from an EEG recording: Delta ($\delta[0.5 \div 4]$Hz), Theta ($\theta[4 \div 8]$Hz), Alpha ($\alpha[8 \div 14]$Hz), Beta ($\beta[13 \div 30]$Hz) and Gamma (over 30Hz). EEG measures, acquired through scalp electrodes placed according to the International 10-20 system (Figure 1), have been widely investigated in the previous century in medical field, mainly to facilitate visual inspection and to extract clinically valuable information. EEG signals present a very high time resolution, which allows dynamic studies to understand the underlying mechanisms by means of complex computational methods. Such a kind of studies has led in recent decades to the use of the brain signal in EEG-based

communication systems, like brain machine interface (BMI) and brain computer interface (BCI), aiming at controlling remote devices by means of brain electrical activity [MW11]. Although early research studies have shown evidence that the EEG carries genetic information, [Vog70], only in the recent years EEG signals have been employed to recognize people within a biometric framework [CRS12]. The interest in using EEG biometrics for automatic person recognition is due to some advantageous peculiarities with respect to other commonly used biometrics, such as privacy compliance, robustness to spoofing attacks and universality. Within this context, EEG recordings have been registered using different acquisition protocols, obtaining promising results in recent works. Some of them rely on the resting state acquisition protocol, which will be the focus of this paper. There is evidence that the electrical activity in resting state condition serves to organize and coordinate neuronal functions [SS01], and it carries genetic information [Vog70]. This has led researchers to further investigate this protocol to extract discriminative information for person recognition purpose, as it is discussed in the following. Specifically, in [PRCE99] 1 channel EEG was collected from 4 subjects performing resting with closed eyes (CE). Ten order AR coefficients in the α band were employed as features. A neural network algorithm yielded a correct classification rate of 95%. A set of 40 users has been employed in [PMBK01], where AR coefficients have been computed to characterize single channel recordings during resting. Discriminant function analysis was used to evaluate data, obtaining a correct classification rate of 82%. Furthermore, in [MSMAS06] Yule-Walker AR parameters of different orders were extracted from the EEG signals of 10 subjects in a resting state. Then a competitive neural network classifier was tested, training on a partition of the dataset and testing on the whole dataset. A correct classification rate of 100% was achieved using sets of 3 channels. Also in [ASLA10] 4 channels EEG recordings were acquired through 4 bipolar measures during resting from 10 subjects. 21 Yule-Walker AR coefficients were extracted using different sets of channels. A neural network algorithm was applied and a correct recognition rate of 97% was achieved for the CE condition, using all channels. Moreover, in [CSB+11] a database of 48 subjects in a CE resting state was acquired from triplets of electrodes. A six order AR model has been estimated for each channel and a polynomial regression based classification has been employed, obtaining a GAR of 96.08%. Spectral features have instead been considered in other EEG biometric systems. In particular, in [MBN08] the fusion of two kind of features, based on the distribution of EEG spectrum in the α band, has been used to verify identities. Signals were acquired by means of one frontal channel, from 23 subjects still resting with closed eyes, achieving a verification rate of 79%. Despite the promising results obtained using the EEG as a biometrics, in all the aforementioned studies a careful analysis aimed at a deep understanding of the underlying phenomena, and at optimizing the parameters involved in the acquisition protocol and successive processing is missing. Therefore in this work we try to fill this gap by focusing on the CE resting state acquisition protocol and speculating on the number of electrodes to use, their spatial configuration, the subbands to analyze, and the AR model order to adopt. The paper is organized as follows. In Section 2 the proposed method is detailed along with the protocol definition, preprocessing, feature extraction, and employed classifier. In Section 3, different sets of electrodes in combination with different subbands are tested for recognition purposes and conclusions are eventually drawn.

神经网络 97%

第二节：提出的方法、预处理、特征提取、分类器

第三节：不同频带导联结合

2 Proposed method

2.1 Experimental setup

To the aim of the proposed analysis, the EEG recordings of $N_C = 45$ healthy volunteers have been acquired. ~~Informed consent was obtained from each subject after the explanation of the study, which was approved by the local institutional ethical committee. During the experiment, the participants were comfortably seated in a reclining chair with both arms resting on a pillow in a dimly lit room properly designed in order to minimize external sounds and noise, not interfering with the attention and the relaxed state of subjects.~~ The subjects were asked to perform one minute of "resting state with closed eyes". Brain activity has been recorded using a BrainAmp recording system operating at a $S_r = 200Hz$ sampling rate, thus producing an $N_T = 200 \times 60$ samples long record for each channel. The EEG was continuously recorded from $C_T = 56$ sites on the scalp, positioned according to the International $10 - 20$ system as shown in Figure 1, and potentials were referenced to the average signal from the ear lobes. Before starting the recording session, the electrical impedance of each electrode was kept lower than 10kOhm through a dedicated gel maximizing the skin contact and allowing for a low-resistance recording through the skin. A set of $N_C = 45$ EEG digital recordings from $C_T = 56$ channels $V_i^{ch}[n]$, for $i = 1, \cdots, N_C$, $n = 1, \cdots, N_T$, and $ch = 1, \cdots, C_T$ has been obtained. The recorded signals have been consequently preprocessed as described in the following Session.

数据采集的过程

200Hz 1分钟
56导联 参考ear lobes

45个人

V:45行代表45个人；56列代表56个导联；第三维长度是200x60代表12000个数据点

2.2 Preprocessing

2.2.1 Downsampling and filtering

The predominant rhythm that can be detected through EEG recordings during wakeful relaxation with closed eyes is composed of α waves ($8 \div 14$Hz), originating from the occipital lobe [BCJ+07]. Nevertheless, also other frequencies still exist, since there isn't any exact frequency the brain is operating on. While resting, resulting EEG patterns contain frequency elements mainly below 30Hz, then the brain rhythms of interest are the δ, θ, α and β waves. In fact the γ subband is known not to be relevant in a resting state. Moreover, we empirically observed a very small signal amplitude over 30Hz, also contaminated by noise such as the 50Hz AC component. In this regard, in a previous work ([CSB+11]) on the use of EEG as biometrics, ratios of the original sampling rate of 200Hz were used to decimate the signal before extracting features. Results showed the most distinctive information to be held below 33 Hz. Given this evidence, in the herein proposed study a more systematic analysis has been carried out in order to properly consider the main EEG waves. In the preprocessing stage a decimation factor has been applied to the collected raw signals. A sampling rate of $S_r = 60$Hz and its anti-aliasing filter were selected, according to the Nyquist theorem, to retain spectral information present in the band $[0.5, 30]$Hz, containing the four major EEG subbands referring to the resting state.

把200Hz的波转换成60Hz？

anti-aliasing filter滤波

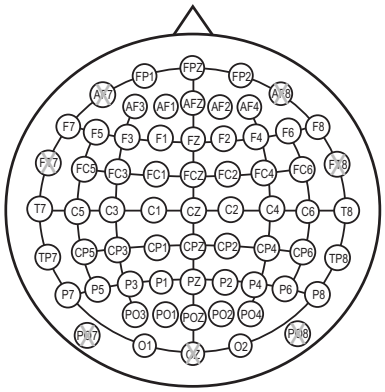

Figure 1: Scalp electrodes positioning according to an extension of the standard 10-20 montage. Electrodes positioning in the employed protocol is shown by the uncrossed circles.

Subsequently, the downsampled signals $V_i^{ch}[n] = V_i^{ch}[n \times 10/3] \mid_{S_r=60}$ has been band-filtered through zero-phase frequency filters to perform the following analysis both for the individual subbands δ, θ, α and β and for their combinations (frequency components from 0.5Hz up to 30Hz, and from 0.5Hz up to 14Hz), obtaining five tested datasets $V_i^{ch}[n] \mid_{Band}$, where $Band \in \{\delta, \theta, \alpha, \beta, [\delta \cup \theta \cup \alpha], [\delta \cup \theta \cup \alpha \cup \beta]\}$. In Figure 2 the spectral maps related to specific frequencies of the different rhythms during resting with closed eyes are displayed in false colors. The strong parieto-occipital α activity at 10Hz can be observed in the related map, while also the spatial distributions on the scalp of other weaker components $(3, 6, 22$Hz) are shown beside.

把这图弄出来应该就能看出降采样的效果咋样

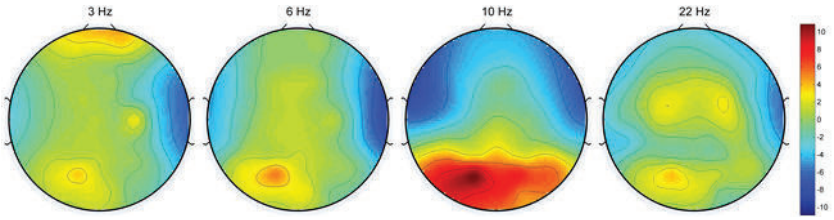

Figure 2: Spectral maps for the CE resting state protocol. The spatial distribution on the scalp of spectral EEG amplitudes at given frequencies, specified above each map, is shown. Each circle represents the top view of a head, where the highest point is the nasion while the lowest is the inion.

空间滤波？

A spatial filter has been then applied to the acquired signals. Specifically, a common average referencing (CAR) filter has been employed by subtracting the mean of the entire electrode montage (*i.e.*the common average) from channels of interest at any one instant. CAR filtering can be applied to reduce artifacts related to inappropriate reference choices in monopolar recordings [SA03] or not expected reference variations, as well as to provide measures as independent as possible from the recording session. This results in an increased SNR, as showed in [MMDW97], where authors compared spatial filter meth-

ods with a conventional ear reference in an EEG-based system. Therefore, in the herein proposed study each channel has been re-referenced to a common average reference composed of all $C_T = 56$ electrodes placed over the entire scalp (see Figure 1) according to the formula:

$$^{CAR}V_i^{ch}[n] = V_i^{ch}[n] - \frac{1}{C_T}\sum_{j=1}^{C_T} V_i^j[n], \tag{1}$$

where $V_i^j[n]$ is the potential between the j-th electrode and the reference electrode. Blink artifact removal, which is customary in EEG signal processing, was not considered in the proposed analysis, since we investigated a CE condition. In this regard we empirically verified that such events are quite absent in the acquired dataset.

CE：close eye

2.2.2 Segmentation and detrend

The so obtained signals are then segmented into M frames. A three second frame length was empirically selected, in order to achieve a trade-off between the sample size and the stationarity of features to be extracted. An overlap interval between adjacent frames was set to increase the sample size. Overlapping percentages of 25%, 50% and 75% of the frame length have been tested. Subsequently the DC component jointly to the linear trend was removed from each EEG segment. The so obtained datasets, $\{^{CAR}V_{i,m}^{ch}\}$, with $i = 1, \cdots, N_C$, $ch = 1, \cdots, C_T$, and $m = 1, \cdots, M$ was further processed to extract the distinctive features from each user brain signal, as described in the following.

2.3 Feature extraction

Given the user i and the channel ch, the generic frame m, $^{CAR}V_{i,m}^{ch}$ is modeled by means of AR stochastic modeling. Specifically the AR reflection coefficients $K_{i,m}^{ch}(Q)$ of order Q have been estimated using the Burg method [Kay88]. The value for the parameter Q has been selected according to the Akaike Information Criterion (AIC), to minimize the information loss in fitting the model according to the formula:

$$\text{AIC}(Q) = N_T \ln \sigma_Q^2 + 2Q \tag{2}$$

being N_T the sequence length, σ_Q^2 the prediction error power, and Q the model order. It has been verified that the AIC(Q) function, averaged among subjects and channels, reaches a plateau zone for values of Q from 8 to12, depending on the considered band. Thus the maximum value of $Q = 12$ has been selected to fit the AR model, so as to satisfy the criterion of minimum information loss for all bands. Hence, for the generic user i, the generic channel ch, the generic frame m, a vector $\boldsymbol{\zeta}_{i,m}^{ch}$ of length Q, composed by the AR model reflection coefficients $K_{i,m}^{ch}(Q)$, for $q = 1, \ldots, Q$, was obtained from each EEG frame $^{CAR}V_{i,m}^{ch}$ with $m = 1, \cdots, M$:

$$\boldsymbol{\zeta}_{i,m}^{ch} = [K_{(i,m)}^{ch}(1), K_{(i,m)}^{ch}(2), \cdots, K_{(i,m)}^{ch}(Q)]^T. \tag{3}$$

Finally, for the i-th user, M features vectors were obtained by concatenating the reflection coefficients vectors related to different sets of channels under analysis. Spatial configura-

tions of $C = 2, 3$ and 5 channels were tested, selecting them with a criteria of symmetry as discussed in Section 3.

2.4 Polynomial Classification

Polynomial based classification [Sch96] was successfully employed for speaker recognition in [CAB02]. In order to classify EEG feature vectors we resort to polynomial based classifiers, which allow to apply a simple linear classification in a properly expanded space, as it is briefly summarized hereafter. Let us denote with $\mathbf{x} = [x_1, \cdots, x_K]^T$ an observed vector, which is supposed to be drawn from a probability distribution belonging to a finite set of cardinality N_C. Lets indicate with $p_{\mathrm{X}|\mathcal{H}_i}(\mathbf{x}|\mathcal{H}_i), i = 1, \cdots, N_C$ the probability density functions describing the N_C not necessarily equiprobable classes or hypotheses $\mathcal{H}_i$, among which to discriminate. Given these assumptions, the classifier we propose estimates the class to which the observed feature vector $\mathbf{x}$ belongs to by means of a linear transformation:

$$\hat{\mathbf{y}}^T(\mathbf{G}) = \mathbf{x}^T \cdot \mathbf{G}, \tag{4}$$

where the matrix $\mathbf{G}$ is obtained by minimizing the mean square error (MMSE), according to the expression:

$$\mathbf{G} = argmin_{\Gamma} \sum_{i=1}^{N_C} P_i \cdot E_{\mathbf{x}|H_i} \left\{ [\mathbf{y}_i - \hat{\mathbf{y}}(\Gamma)]^T [\mathbf{y}_i - \hat{\mathbf{y}}(\Gamma)] \right\}. \tag{5}$$

Here, assuming the hypothesis $\mathcal{H}_i$ holds, the vector $\mathbf{y}_i = [0, \ldots, 0, 1, 0, \ldots, 0]$ with the unique one in the i-th position, indicates the class i $\mathbf{x}$ belongs to, while $\hat{\mathbf{y}}(\mathbf{G})$ represents its estimation. $\mathcal{P}_i$ denotes the (prior) probability that $\mathbf{x}$ belongs to the i-th class. It can be easily shown that the employed optimization criterion given in (5) brings to the normal equations:

$$\mathbf{R}_{\mathrm{x}} \cdot \mathbf{G} = \mathbf{R}_{\mathrm{xy}}, \tag{6}$$

where $\mathbf{R}_{\mathrm{x}} = \mathrm{E}\left\{\mathbf{x}\mathbf{x}^T\right\}$ is the classical matrix collecting the (auto)-correlations established intra the elements of the observation vector $\mathbf{x}$, while $\mathbf{R}_{\mathrm{xy}} = \sum_{i=1}^{N_C} \mathcal{P}_i \cdot E_{x|\mathcal{H}_i}\{\mathbf{x}\} \cdot \mathbf{y}_i^T$. It is worth noting that (4) states that decision regions are formed through plane intersections in the space of the observations $\mathbf{x}$. This is non optimal, since the boundary of the decision regions are nonlinear curves whose forms depend on the actual probability density functions at hand. The approximation through a polynomial regression of these boundaries still allows to retain the linear classification form (4), but letting this latter rather operate on a suitably nonlinearly expanded observations space $\mathbf{z}$ with increased cardinality. Specifically, given the observation vector $\mathbf{x} = [x_1, \cdots, x_K]^T$, its polynomial expanded counterpart consists of a constant unit term, followed by K linear terms x_m, followed by all the quadratic terms, followed by all the cubic terms and so forth. For instance, the complete polynomial expansion up to the third order of $x = [x_1, x_2]$ yields the following expanded vector: $\mathbf{z}(\mathbf{x}) = [1, x_1, x_2, x_1^2, x_1x_2, x_2^2, x_1^3, x_1^2x_2; x_1x_2^2; x_2^3]^T$. The D-degree polynomial expansion of a K-vector yields a $K_D = \binom{k+D}{D}$ vector. When operating on a polynomial expanded vector, the linear classifier (4) is written as follows: $\hat{\mathbf{y}}^T(\mathbf{G}) = \mathbf{z}(\mathbf{x})^T\mathbf{G}$, with

$$\mathbf{R}_{\mathrm{z}} \cdot \mathbf{G} = \mathbf{R}_{\mathrm{zy}}. \tag{7}$$

2.4.1 Dataset

As described in Section 2.3, features vectors $\boldsymbol{\zeta}$ to be classified have been extracted considering the combination of different sets of $C = 2, 3$ and 5 symmetrically placed channels which have been listed in Tables 1, 2 and 3. Given a chosen set of channels, each of the acquired signals have been pre-processed as described in Section 2.2, segmented into M frames, and modeled by means of the reflection coefficients of an AR model of order Q, obtaining the set of vectors $\boldsymbol{\zeta}_{i,m}^{ch}$. More in detail, the acquired EEG signals of duration of $60s$, have been segmented into frames of $3s$, with an overlap factor of 75%, thus obtaining a number of $M = 77$ frames, each of which is represented by the vector $\boldsymbol{\zeta}_{i,m}$ of $Q \times C$ elements, being the concatenation of the C vectors $\boldsymbol{\zeta}_{i,m}^{ch}$. Such a set of vectors $\boldsymbol{\zeta}_{i,m}$ for $i = 1, \cdots, N_C$ and $m = 1, \cdots, M$, has been extracted for all the 6 bands of interest (see Section 2.2). Therefore, an identification framework has been provided, as described in the following.

2.4.2 Training and identification

It is worth pointing out that datasets have been assorted in order not to have overlapping between the ones used in the training stage and the ones used in the recognition stage. Specifically, the first consecutive $M_T = 2M/3$ frames have been used to assort the training dataset and the last $M_C = M/3$ ones to assort the testing dataset. Moreover, the overlapping frames containing samples common to the two datasets have removed to provide disjointed sets. The training stage consists in the estimation of the matrix $\mathbf{G}$ in (7) computed as $\mathbf{G} = \widehat{\mathbf{R}}_{\mathrm{z}}^{-1} \cdot \widehat{\mathbf{R}}_{\mathrm{zy}}$, where the matrices $\mathbf{R}_{\mathrm{z}}$ and $\mathbf{R}_{\mathrm{zy}}$ are estimated through MonteCarlo runs, considering equal prior probabilities $\mathcal{P}_i$ for all the considered classes. The estimation was obtained performing the following two sample averages:

$$\widehat{\mathbf{R}}_{\mathrm{z}} = \frac{1}{N_C M_T} \sum_{i=1}^{N_C} \sum_{m=1}^{M_T} \mathbf{z}_{i,m} \mathbf{z}_{i,m}^T; \; \widehat{\mathbf{R}}_{\mathrm{zy}} = \frac{1}{N_C M_T} \sum_{i=1}^{N_C} \sum_{m=1}^{M_T} \mathbf{z}_{i,m} \mathbf{y}_i^T, \tag{8}$$

where $\mathbf{z}_{i,m}$ is the expansion of the m-th observed feature vector $\boldsymbol{\zeta}_{i,m}$ belonging to the i-th class, where $\mathbf{y}_i = [0, \ldots, 0, 1, 0, \ldots, 0]^T$, with the unique 1 in the i-th position. A $D = 2$ degree polynomial regression has been employed to perform a linear classification in the nonlinearly expanded observations space $\mathbf{z}$. This value for the polynomial degree was selected in order to contain the increased cardinality considering the actual length of the features vector $\boldsymbol{\zeta}$. In fact, to properly estimate the matrix $\widehat{\mathbf{R}}_{\mathrm{z}}$, whose dimensions are $[K_D \times K_D]$, a number of MonteCarlo runs $N_C \times M_T \geq K_D$ are needed. To avoid failures and to control accuracy in the estimation of $\mathbf{R}_{\mathrm{z}}^{-1}$, the singular value decomposition based pseudoinversion has been used for the matrix inversion.

In the classification stage, for each of the N_C users, a common averaging is applied to the M_C observed features vectors from the test dataset. For the i-th user a score vector $\hat{\mathbf{y}}_i$ is obtained for each mean vector $\overline{\boldsymbol{\zeta}}_i = 1/M_T \sum_{m=1}^{M_T} \boldsymbol{\zeta}_{i,m}$, applying the discrimination matrix $\mathbf{G}$ to $\overline{\boldsymbol{\zeta}}_i$: $\hat{\mathbf{y}}_i = \mathbf{G} \cdot \overline{\boldsymbol{\zeta}}_i$. Finally the estimation of the user index is obtained locating the maximum of the score vector $\hat{\mathbf{y}}_i = [\hat{y}_i(1), \ldots, \hat{y}_i(N_C)]^T$ according to the criterion $\hat{i} = \arg_l \max y_i(l)$.

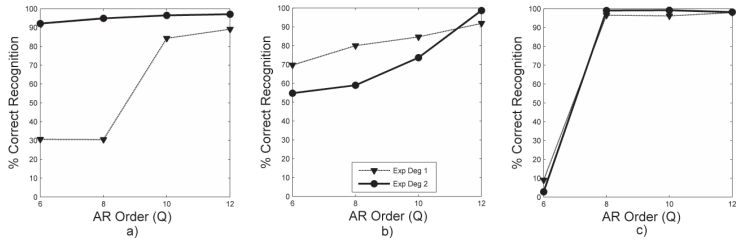

Figure 3: Recognition performance *vs* AR order model, with overlap factor of 75% for: a) best couple; b) best triplet; c) best set of five 5 electrodes.

3 Experimental results and conclusions

A systematic analysis of all the involved parameters has been here performed on the EEG signals acquired from 45 healthy subjects using a "resting state with closed eyes" protocol. Specifically, given the 56 employed channels shown in Figure 1, we have considered different subsets of them in order to find the best performing spatial arrangements of electrodes while minimizing their number. To achieve this goal we have considered sets of two, three, and five electrodes, listed in Tables 1, 2 and 3. Symmetrical configurations have been selected, spanning the entire scalp for sets of two and three channels (Tables 1 and 2), while considering only the central-posterior areas for sets of 5 electrodes (Table 3). AR modeling has been employed to extract the feature vectors from EEG recordings, which have been first preprocessed as described in Section 2.2. In this stage signals have been decimated with sampling rate of 60 Hz, in order to maintain the frequency components in the range of interest $[0 - 30\text{Hz}]$, and band pass filtered to further extract and analyze the brain rhythmic activity in the bands δ, θ, α and β and in some of their combinations. A spatial filter has been then employed to improve the SNR, controlling artifacts that may occur on the single reference electrode. Furthermore, the so obtained signals have been normalized, segmented into overlapping frames of T_fs with an overlapping factor O_L between consecutive frames, and the linear trend has been removed. Values of $T_f = 3s$, and $O_L = 75\%$ have been selected in order to capture locally stationary and repeatable features, while providing a proper number of frames to train the classification algorithm. In fact we have experimentally verified that increasing the dataset size through the overlapping factors of 25% 50% and 75%, leads to improved performance due to a better estimation of the matrices involved in the classification algorithm. A number of $M = 77$ frames has been obtained, and AR reflection coefficients have been estimated from each of them to generate features vectors. The order $Q = 12$ of the AR model has been properly estimated using the AIC [Kay88], but different orders $Q \in \{6, 8, 10, 12\}$ have been tested providing an experimental validation of the adopted model in terms of performance. In Figure 3 it can be observed that increasing the model order up to $Q = 12$ leads to improved performance for all the considered sets of channels. For each frame a template is obtained by concatenating the reflection coefficients referring to the signals from the electrodes set under analysis, thus generating feature vectors of length $24, 48, 60$

electrodes	$\delta \cup \theta \cup \alpha \cup \beta$	$\delta \cup \theta \cup \alpha$	δ	θ	α	β
Fp1 Fp2	77.66	73.54	54.34	40.75	56.05	22.80
AF3 AF4	83.67	78.44	57.00	43.38	57.86	24.10
F7 F8	81.18	79.48	56.28	35.99	59.02	23.84
FC5 FC6	90.33	79.88	61.79	44.33	63.64	26.84
FC3 FC4	90.91	82.94	56.16	44.99	61.21	32.03
FC1 FC2	90.39	78.35	59.71	40.89	61.15	28.51
T7 T8	91.52	84.04	68.28	54.17	65.37	35.56
C5 C6	89.73	76.25	58.90	44.33	62.40	32.53
C3 C4	90.71	83.64	59.37	48.31	60.52	36.19
C1 C2	93.16	76.45	57.17	44.33	62.28	37.60
TP7 TP8	89.18	82.16	64.59	55.12	67.99	29.99
CP5 CP6	86.41	79.28	60.06	47.36	56.97	28.17
CP3 CP4	90.48	74.14	63.92	49.06	58.21	33.04
CP1 CP2	86.12	70.76	56.05	41.33	54.89	29.81
P7 P8	91.98	84.44	70.79	58.07	69.61	39.08
P5 P6	94.26	80.58	68.34	53.02	66.64	28.48
P3 P4	92.09	82.71	62.74	51.40	67.76	27.13
P1 P2	90.65	81.15	59.71	46.52	66.12	30.68
PO3 PO4	96.57	87.65	77.58	62.83	72.70	38.61
O1 O2	95.41	87.59	72.73	56.57	74.60	41.10
F5 F6	84.10	83.15	55.18	42.22	60.52	26.55
F3 F4	86.58	80.23	61.15	43.81	59.68	32.67
F1 F2	87.50	73.22	52.01	45.11	57.03	30.04
Fpz AFz	86.15	73.28	58.99	44.18	59.51	29.47
AFz Fz	88.83	79.08	61.15	42.94	56.59	26.23
Fpz Cz	93.19	85.08	69.21	53.25	67.13	33.25
Fpz FCz	91.86	88.23	70.74	55.21	66.61	33.07
Fpz Fz	89.55	82.57	62.74	54.92	62.37	31.08
Fpz CPz	88.92	83.55	65.66	51.72	64.50	33.02
Fpz Pz	88.98	83.41	64.88	51.98	68.57	30.68
Fpz POz	89.73	84.82	72.90	57.84	68.92	34.92
AFz FCz	93.51	85.22	67.91	48.95	65.48	32.18
AFz Cz	94.52	82.37	66.87	52.18	69.47	34.83
AFz CPz	89.90	81.04	64.56	50.71	68.11	35.61
AFz Pz	91.28	84.13	64.39	44.99	70.07	34.57
AFz POz	91.89	84.56	72.73	51.86	71.20	42.97
Fz FCz	91.60	80.72	59.16	45.83	56.39	26.00
Fz Cz	95.32	85.89	66.03	53.30	62.91	36.22
Fz CPz	92.78	85.22	62.68	56.02	66.06	38.27
Fz Pz	93.77	86.81	64.73	48.66	68.63	35.21
Fz POz	95.24	89.03	74.34	55.84	69.75	43.64
FCz Cz	96.59	88.23	65.02	51.23	57.63	37.60
FCz CPz	94.49	90.25	71.72	58.99	66.23	36.71
FCz Pz	95.12	88.77	73.28	55.30	75.47	37.20
FCz POz	97.09	90.07	76.68	59.51	75.18	41.10
Cz CPz	91.11	80.32	64.99	47.07	62.16	37.17
Cz Pz	93.65	86.32	68.66	55.79	71.40	39.62
Cz POz	94.89	85.89	77.66	56.05	73.02	35.93
CPz Pz	91.66	81.99	62.25	53.82	63.12	35.44
CPz POz	92.87	88.95	73.56	58.44	71.14	40.32
Pz POz	90.22	83.75	69.87	47.79	66.61	32.53

Table 1: Classification results in % obtained for the subbands δ, θ, α, β, and the fusions $\delta \cup \theta \cup \alpha \cup \beta$ and $\delta \cup \theta \cup \alpha$ for sets of two electrodes. $O_L = 75\%, Q = 12$.

electrodes	$\delta \cup \theta \cup \alpha \cup \beta$	$\delta \cup \theta \cup \alpha$	δ	θ	α	β
Fp1 Fpz Fp2	79.65	78.47	58.96	45.69	58.61	26.26
AF3 AFz AF4	88.25	80.55	63.35	45.25	63.64	26.64
F7 Fz F8	92.76	89.61	70.97	55.44	71.28	31.75
FC5 FCz FC6	95.56	89.93	74.57	62.86	78.93	39.97
T7 Cz T8	97.75	92.70	81.62	72.67	83.61	47.42
C5 Cz C6	96.57	89.81	80.58	62.05	77.14	41.24
C3 Cz C4	97.52	92.70	75.90	67.01	73.42	47.01
C1 Cz C2	95.50	82.57	65.66	52.09	66.67	45.54
TP7 CPz TP8	95.70	90.22	79.54	68.72	78.15	46.18
P7 Pz P8	96.51	90.10	79.45	67.33	81.76	49.96
PO1 POz PO2	95.04	88.54	78.33	57.32	76.57	45.95
PO3 POz PO4	98.10	93.04	84.68	71.14	84.91	51.66
O1 POz O2	98.73	90.59	77.37	61.41	84.79	53.88

Table 2: Classification results in % obtained for the subbands δ, θ, α, β, and the fusions $\delta \cup \theta \cup \alpha \cup \beta$ and $\delta \cup \theta \cup \alpha$ for sets of three electrodes. $O_L = 75\%, Q = 12$.

for the sets of two, three, and five electrodes respectively. A polynomial classifier has been then employed using an expansion factor $D = 2$. It is worth pointing out that the expansion factor has been kept low, since, given the dimension of the feature vector considered in this paper, a higher expansion factor would lead to a dimensionality curse resulting in heavy computational load and matrices estimation problems. In Figure 3 it is shown the comparison between recognition performances obtained employing a simple linear classifier based on the MMSE and a 2-degree polynomial classifier. Results showed that best performance of 97.09% and 98.73% has been obtained setting $Q = 12$ and $D = 2$ for sets of two and three channels respectively, while remaining below 90% for $D = 1$. Referring to sets of five channels it should be noticed that the space expansion doesn't provide significant improvements in the recognition performance. In this case a correct recognition rate of about 99% is obtained for $Q = 10, 12$ and $D = 2$, which differs not significantly from the best performance achieved by using three channels, while requiring an inconvenient greater number of electrodes. Finally, a cross-validation framework has been provided for all the considered sets of channels and frequency bands, obtaining results shown in Tables 1, 2, and 3. The set of frames used for training and test have been kept disjoint. It should be noticed that the channel spatial configurations giving the best performance have been proven to be located mainly in the parieto-occipital area PO of the scalp (O1-POz-O2, PO3-POz-PO4, Cz-TP7-CPz-TP8-Pz, Cz-P7-CPz-TP8-Pz), while the worst performing sets of electrodes are placed in the fronto-polar region FP (FP1-FP2, FP1-FPz-FP2). This is in agreement with the experimental finding that α and β rhythms carry individual-specific traits, claimed to be genetically induced [VPR91], and with the observation that the oscillatory α activity is the most dominant rhythm which emerges from the PO region in a condition of relaxation with closed eyes [BCJ$^+$07], corresponding with the herein employed experimental protocol. According to this evidence, the most considerable contribution to the correct recognition performance, for the given dataset, comes from the α band followed by the β band, as it can be observed comparing the column 3 of each table to the columns 4, 5 and 6. Moreover, as it can be observed in Figure 2, the worst performing FP region doesn't show α activity, while it is strongly detected

electrodes	$\delta \cup \theta \cup \alpha \cup \beta$	$\delta \cup \theta \cup \alpha$	δ	θ	α	β
FCz T7 Cz T8 CPz	97.84	94.34	86.20	76.10	84.99	57.32
FCz C5 Cz C6 CPz	97.23	94.55	83.55	65.28	77.17	48.83
FCz C3 Cz C4 CPz	98.07	90.68	80.14	72.09	74.43	51.40
FCz C1 Cz C2 CPz	96.91	83.90	72.06	55.93	65.25	46.38
Cz TP7 CPz TP8 Pz	98.56	94.75	84.16	74.86	84.91	53.65
Cz CP5 CPz CP6 Pz	97.20	92.50	79.54	67.53	79.62	45.37
Cz CP3 CPz CP4 Pz	96.83	91.86	79.45	66.90	78.70	51.08
Cz CP1 CPz CP2 Pz	96.16	86.98	67.73	51.20	73.19	43.20
CPz P7 Pz P8 POz	97.20	92.44	84.33	71.83	83.98	51.20
CPz P5 Pz P6 POz	97.92	93.13	82.16	65.28	84.73	48.60
CPz P3 Pz P4 POz	97.52	90.39	76.80	62.37	83.26	43.32
CPz P1 Pz P2 POz	97.29	89.64	72.15	53.45	75.38	36.19
Pz PO3 PO4 O1 O2	98.21	92.06	79.57	70.10	83.15	52.50

Table 3: Classification results in % obtained for the subbands δ, θ, α, β, and the fusions $\delta \cup \theta \cup \alpha \cup \beta$ and $\delta \cup \theta \cup \alpha$ for sets of five electrodes. $O_L = 75\%, Q = 12$.

in the PO area. Besides, eyes movement artifacts mostly affect the FP region, due to the proximity of the involved muscles.

In conclusion, our analysis achieves more accuracy compared with the works investigating the CE condition cited in Section 1, especially considering the size of the employed datasets and the separation of the training and the test datasets. A better result is obtained also respect to other acquisition protocols, such as open eyes condition in [ASLA10]. Our contribution concerns the investigation of the most characteristic combination of subbands to analyze, the proper segmentation and spatial configuration of electrodes to employ, while using an efficient polynomial regression classifier. It proves that a preliminary data screening is needed for the optimal setting of the involved parameters. Our extensive analysis has shown that, within the employed classification framework, the α rhythm can be successfully employed for recognition purposes, since the used acquisition protocol and the proper choice of the electrodes number and their positioning allowed reaching recognition rates equal almost to 99% through a second order polynomial regression.

Acknowledgments

The authors are grateful to prof. F. Babiloni for having provided the test set.

References

[ASLA10] M.K. Abdullah, K.S. Subari, J.L.C. Loong, and N.N. Ahmad. Analysis of effective channel placement for an EEG-based biometric system. In *Proc. IEEE EMBS Conf. Biomed. Eng. Sci. (IECBES)*, pages 303–306, 2010.

[Baş99] E. Başar. *Brain Function and Oscillations: Integrative brain function. Neurophysiology and cognitive processes*. Springer, 1999.

[BCJ+07] R.J. Barry, A.R. Clarke, S.J. Johnstone, C.A. Magee, and J.A. Rushby. EEG differences between eyes-closed and eyes-open resting conditions. *Clinical Neurophysiology*, 118:2765–2773, 2007.

[Ber29] Hans Berger. Über das Elektrenkephalogramm des Menschen. *European Archives of Psychiatry and Clinical Neuroscience*, 87:527–570, 1929.

[CAB02] W.M. Campbell, K.T. Assaleh, and C.C. Broun. Speaker Recognition with Polynomial classifiers. *IEEE Trans. Speech Audio Process.*, 10:205–212, 2002.

[CRS12] P. Campisi, D. La Rocca, and G. Scarano. EEG for Automatic Person Identification. *IEEE Computer*, (7), 2012.

[CSB+11] P. Campisi, G. Scarano, F. Babiloni, F. DeVico Fallani, S. Colonnese, E. Maiorana, and L. Forastiere. Brain waves based user recognition using the eyes closed resting conditions protocol. In *IEEE Int. Workshop Inf. Foren. Sec. (WIFS)*, pages 1–6, 2011.

[Kay88] S.M. Kay. *Modern Spectral Estimation. Theory and Applications*. Prentice-Hall, 1988.

[MBN08] C. Miyamoto, S. Baba, and I. Nakanishi. Biometric person authentication using new spectral features of electroencephalogram (EEG). In *Int. Symp. Intell. Signal Process. Commun. Syst. (ISPACS)*, pages 1–4, 2008.

[MMDW97] D. McFarland, L. McCane, S. David, and J. Wolpaw. Spatial filter selection for EEG-based communication. *Electroencephalography and Clinical Neurophysiology*, 103:386–394, 1997.

[MSMAS06] G. Mohammadi, P. Shoushtari, B. Molaee Ardekani, and M. B. Shamsollahi. Person Identification by Using AR Model for EEG Signals. In *Proc. Of World Academy of Sic. Eng. And Tech.*, volume 11, pages 281–285, 2006.

[MW11] D.J. McFarland and J.R. Wolpaw. Brain-computer interfaces for communication and control. *Commun. ACM*, 54:60–66, 2011.

[PMBK01] R.B. Paranjape, J. Mahovsky, L. Benedicenti, and Z. Koles. The electroencephalogram as a biometric. In *Canadian Conf. on Elec. & Comp. Eng.*, pages 1363–1366, 2001.

[PRCE99] M. Poulos, M. Rangoussi, V. Chrissikopoulos, and A. Evangelou. Person identification based on parametric processing of the EEG. In *The 6th IEEE Int. Conf. on Electronics, Circuits and Systems (ICECS)*, volume 1, pages 283–286, 1999.

[SA03] M.S. Schwartz and F. Andrasik. *Biofeedback: A Practitioner's Guide*. Guilford Press, 2003.

[Sch96] J. Schurmann. *Pattern Classification: A Unified View Of Statistical And Neural Approaches*. Wiley, 1996.

[SS01] E. Salinas and T.J. Sejnowski. Correlated Neuronal Activity and the Flow of Neural Information. *Nature Reviews Neuroscience*, 2:539–550, 2001.

[Vog70] F. Vogel. The genetic basis of the normal human electroencephalogram (EEG). *Humangenetik*, 10(2):91–114, 1970.

[VPR91] J.L. Varner, R.A. Potter, and J.W. Rohrbaugh. A Procedure For Automatic Classification Of EEG Genetic Variants. In *Proc. of the IEEE Eng. in Medicine and Biology Soc. (EMBS)*, volume 13, pages 451–452, 1991.